Published in final edited form as:
Cancer Res. 2010 November 15; 70(22): 9319–9328. doi:10.1158/0008-5472.CAN-10-1783.

Synergistic Enhancement of Carboplatin Efficacy with Photodynamic Therapy in a Three-dimensional Model for Micrometastatic Ovarian Cancer

Imran Rizvi[‡,†], **Jonathan P. Celli**[‡], **Conor L. Evans**[‡], **Adnan O. Abu-Yousif**[‡], **Alona Muzikansky**[§], **Brian W. Pogue**[†], **Dianne Finkelstein**[§], and **Tayyaba Hasan**[‡,*]

[‡]Wellman Center for Photomedicine, Massachusetts General Hospital, Harvard Medical School, Boston, Massachusetts 02114

[†]Thayer School of Engineering, Dartmouth College, Hanover, New Hampshire 03755

[§]Biostatistics Center, Massachusetts General Hospital, Boston, Massachusetts 02114

Abstract

Metastatic ovarian cancer frequently recurs due to chemoresistance, highlighting the need for non-overlapping combination therapies that mechanistically synergize to eradicate residual disease. Photodynamic therapy (PDT), a photochemistry-based cytotoxic modality, sensitizes ovarian tumors to platinum agents and biologics, and has shown clinical promise against ovarian carcinomatosis. We introduce a three-dimensional model representing adherent ovarian micrometastases and high-throughput quantitative imaging methods to rapidly screen the order-dependent effects of combining benzoporphyrin derivative monoacid-A (BPD)-based PDT with low-dose carboplatin. Three-dimensional ovarian micronodules grown on Matrigel™ were subjected to BPD-PDT either before or after carboplatin treatment. We developed custom fluorescence image analysis routines to quantify residual tumor volume and viability. Carboplatin alone did not eradicate ovarian micrometastases at a dose of 400 mg/m^2, leaving surviving cores that were non-sensitive or impermeable to chemotherapy. BPD-PDT (1.25μM·J/cm^2) created punctate cytotoxic regions within tumors and disrupted micronodular structure. Treatment with BPD-PDT prior to low-dose carboplatin (40 mg/m^2), produced a significant synergistic reduction (p<0.0001 ANCOVA) in residual tumor volume (0.26, 95% confidence interval (CI)=0.19-0.36), compared to PDT alone (0.76, 95% CI=0.63-0.92) or carboplatin alone (0.95, 95% CI=0.83-1.09), relative to controls. This synergism was not observed with the reverse treatment order. Here, we demonstrate for the first time the use of a 3D model for micrometastatic ovarian cancer as a rapid and quantitative reporter to optimize sequence and dosing regimens of clinically relevant combination strategies. This approach combining biological modeling with high-content imaging provides a platform to rapidly screen therapeutic strategies for a broad array of metastatic tumors.

INTRODUCTION

The vast majority of ovarian cancer (OvCa) cases are diagnosed once the disease has metastasized to distant sites, which substantially diminishes the possibility of providing curative treatments (1-4). Despite advancements in surgical debulking techniques, optimization of chemotherapeutic regimens, and improvements in radiotherapy, five-year progression-free survival (PFS) and overall survival (OS) rates remain low, even among

*Address all correspondence to: Wellman Center for Photomedicine, Massachusetts General Hospital, 40 Blossom St, Boston, MA 02114. thasan@partners.org.

women whose disease is optimally cytoreduced to ≤1cm in diameter (1,5). These results indicate that unresected tumor nodules respond poorly to traditional agents, due primarily to poor drug penetration (6,7) and the development of resistance (8-10). There is a critical need to design and rapidly evaluate more effective management strategies for residual OvCa. Identifying the most promising treatments among the vast library of candidate agents has been a slow and unreliable process due, in part, to a lack of high-throughput model systems that capture critical aspects of tumor biology (1,11,12). We address this limitation, by developing an *in vitro* three-dimensional (3D) model for adherent micrometastatic OvCa, which in conjunction with custom image analysis routines designed in our group, serves as a high-throughput reporter for treatment efficacy. We use this platform to evaluate a mechanism-based combination regimen that synergistically enhances carboplatin efficacy with photodynamic therapy (PDT), a photophysical cytotoxic modality that sensitizes OvCa cells to chemo and biologic agents (4,13), and has shown promise in clinic trials for the treatment of ovarian carcinomatosis (14-19).

Rationally designed combination therapies provide the best hope of improving outcomes for patients with advanced stage disease, by exploiting non-overlapping cellular targets, improving drug transport and mitigating the survival signals that lead to treatment resistance (1,4,8,13,20-22). agents has been a longstanding clinical approach that has modestly improved initial response rates in patients with advanced stage OvCa (2,9,10,23). Despite improvements with combining chemotherapies, rates of recurrence remain as high as 80% (8,9), indicating that traditional chemotherapies by themselves hold little promise of having a significant impact on PFS and OS (8,9).

We (4,13) and others (21,22) have shown that PDT-based combination regimens sensitize tumors, including OvCa, to chemotherapeutics and targeted biological inhibitors. PDT involves activation of a photosensitive molecule by light of a specific wavelength to generate reactive species (18,21,24-29), and is approved for a variety of applications including actinic keratosis, non-small cell lung cancer and palliation of obstructive esophageal cancer using Photofrin (24,26). PDT is also approved globally as a first-line therapy for age-related macular degeneration (24) using benzoporphyrin-derivative monoacid ring A (BPD-MA, verteporfin), which offers better photobiologic activity and shorter cutaneous phototoxicity than Photofrin (4,29-31).

BPD also provides promising results for the treatment of multifocal OvCa (4,31,32). We have reported that BPD-PDT combined with Erbitux®, an antibody that targets the epidermal growth factor receptor (EGFR), synergistically reduces tumor burden and enhances survival in a mouse model for ovarian carcinomatosis (4). Combining these mechanistically-distinct monotherapies mitigates the limitations of each modality (4). Molpus et al. showed that multiple cycles of BPD-PDT were required to achieve therapeutic benefit in a murine model for ovarian carcinomatosis (31). Erbitux, a cytostatic therapy, is administered at high doses for extended periods with modest improvements in survival (33). Combining BPD-PDT with Erbitux improved acute and long-term therapeutic outcomes, with fewer treatment cycles and minimal toxicity (4). These promising results have informed large animal studies leading to clinical trials using BPD-PDT in combination with Erbitux to treat metastatic OvCa (32).

In a variant of this approach, photoimmunotherapy (PIT), chlorin e_6 was conjugated to a monoclonal antibody, OC125, creating a therapeutically active targeting moiety (13). In cisplatin resistant tissue, PIT reversed chemoresistance and produced a synergistic 12.9-fold increase in cytotoxicity compared to cisplatin alone. The combination treatment had an additive effect in cisplatin sensitive tissue. Among all patient tissue samples and cell lines, PIT increased OvCa sensitivity to cisplatin by 6.9-fold, compared to cisplatin alone (13).

Here we introduce an *in vitro* 3D tumor model for adherent, micrometastatic OvCa, adapted from breast cancer models (34,35), as a treatment response platform to efficiently evaluate combination therapies. These ovarian 3D tumors represent unresectable, multifocal micronodules that are typically managed with chemotherapy and are precursors to recurrent metastatic disease (1-3). We use this biological and imaging-based platform to determine the effect of combining BPD-PDT and carboplatin. We hypothesized that the interaction between these mechanistically-distinct cytotoxic modalities would lead to synergistic enhancement of the monotherapies. Our results show that carboplatin alone does not eradicate OvCa at clinically relevant doses, and demonstrate for the first time a sequence-dependent synergistic enhancement of carboplatin efficacy by BPD-PDT in a 3D model for micrometastatic OvCa.

MATERIALS AND METHODS

Cell lines and culture

NIH:OVCAR-5 human epithelial OvCa cells were obtained from Thomas Hamilton (Fox Chase Cancer Institute, Philadelphia, PA), and previously characterized by microsatellite marker analysis. Cells were maintained as previously described (4).

Monolayer Cultures—OVCAR5 cells were plated in 35 mm dishes (#353001; BD Biosciences; Franklin Lakes, NJ) at a density of 210,000 cells in 2 ml media.

Three-dimensional (3D) Cultures—Protocols for 3D ovarian cultures were adapted from previously published methods for breast cancer cell lines (34,35). Briefly, 150μl or 250μl Growth Factor Reduced-Matrigel™ (GFR-Matrigel) (#354230; BD Biosciences; Franklin Lakes, NJ) was pipetted into the center well of a chilled 35mm MatTek dish (P35G-0-20-C; MatTek Corp.; Ashland,MA), or each well of a black-walled 24-well plate (Genetix W1350). An OVCAR5 cell suspension (500μL of a 1.5×10^4 cells/ml) was pipetted onto each dish/well. After 30 minutes media was added to a final concentration of 2% GFR-Matrigel, and changed every 2-3 days.

Growth Characterization

Darkfield microscopy images (5 fields per culture per timepoint) were acquired using an inverted microscope (Zeiss Axiovert 100 TV, Zeiss, Germany) with a CCD camera (Quantifire XI, Optronix, Israel) and saved as uncompressed TIFFs. Image data was batch processed using custom MATLAB (Mathworks, Natick, MA) routines to report equivalent diameters of automatically segmented (nearly) circular regions corresponding to 3D nodules as previously described (36). *N* values represent individual 3D culture dishes and standard deviations report the reproducibility of mean diameter from independent platings. Timelapse 10X phase contrast sequences were obtained using a microscope (TE2000-S, Nikon) in a weatherstation (37°C, 5% CO_2).

Immunofluorescence Protocol

A previously established immunofluorescence protocol was used(37). Human fibronectin (Sigma F0916) and mouse anti-E-cadherin (Transduction Laboratories C20820) antibodies were fluorescently labeled using Alexa-$Fluor_{568}$ goat anti-mouse secondary antibodies (A11004, Invitrogen). DAPI (4′,6-diamidino-2-phenylindole) (Sigma 32670) was diluted 1:1000 in PBS to stain nuclei.

Treatments

Carboplatin—To establish dose response in monolayer versus 3D, cultures were treated with 0.4 to 400 mg/m^2 carboplatin in either standard media (monolayer) or standard media with 2% GFR-Matrigel (3D media). Cytotoxicity was evaluated following either a 24 hour incubation in monolayer or 96 hour incubation in 3D cultures. Carboplatin treatments for all combination therapy experiments were initiated on day 10 post-plating, and terminated on day 14 using a dose of 40 mg/m^2, to keep the carboplatin dose and incubation period fixed for both treatment sequences.

Photodynamic therapy (PDT)—Cultures were incubated with 250nM BPD-MA (QLT, Inc., Vancouver, BC, Canada) for 90 minutes in standard media. Immediately prior to irradiation, BPD-MA media was replaced with either fresh standard media (monolayer cultures) or standard media with 2% GFR-Matrigel (3D cultures). Each dish/well was irradiated with a 690nm fiber coupled diode laser (Model 7401; High Power Devices, Inc., North Brunswick, NJ, USA) at a fluence rate of 40mW/cm^2 (VEGA Laser Power Energy Meter, Ophir Laser Measurement Group, LLC, North Logan, UT). For monolayer versus 3D culture experiment, fluences of 0.1, 1.0, 2.5, or 5.0J/cm^2 were delivered, for total PDT doses ([PS] × fluence) of 0.025, 0.25, 0.625 and 1.25 μM·J/cm^2, respectively. To determine sequence-dependent cytotoxic response in combination therapy experiments, 3D cultures were treated with 1.25 μM·J/cm^2 BPD-PDT on either day 10 or day 14 post-plating (prior to, or upon completion of, carboplatin treatment, respectively).

Controls were subjected to sham manipulations. *N* values for treatment studies represent individual 3D cultures over a minimum of three independent platings.

High-throughput fluorescence imaging and cytotoxicity analysis

Cultures were incubated with LIVE/DEAD™ reagents (Invitrogen, L-3224) Calcein AM (live) and ethidium bromide (dead) which overcome limitations of MTT and MTS that bind to GFR-Matrigel™. Using an Olympus FV-1000 confocal microscope with automated stage, multichannel fluorescence images from multiwell dishes were acquired in high-throughput using a 4X objective (488nm excitation, with FITC emission filter and 559nm excitation, with TRITC emission filter for calcein and ethidium homodimer-1, respectively). Laser and photomultiplier tube settings, optimized for maximum dynamic range, were internally consistent across experimental groups.

Therapeutic efficacy was quantified by two metrics: 1.) Residual tumor volume, a measure of how much viable disease remains on each plate; and 2.) Tumor viability, a ratiometric quantification of how viable the residual disease is. Image datasets were batch-processed using custom MATLAB routines (36). Calcein images were segmented (as above) to calculate nodule volumes from equivalent diameters, d_{eq}, by, $V=\frac{4}{3}\pi\left(\frac{d_{eq}}{2}\right)^3$ and then summed to determine total volume reported as fraction of the no-treatment control. Tumor viability was quantified by the ratio of calcein to total fluorescence intensity (calcein plus ethidium) and normalized to no-treatment as previously described (36).

Statistical Analysis

For each experiment, we fit analysis of covariance (ANCOVA) models for the effect from each intervention (PDT, carboplatin and the combination treatments), adjusting for batch and day (which ensured that the proper control group was used for the comparison). In order to keep the carboplatin dose and schedule fixed for both treatment sequences, the timepoints for PDT treatment and cytotoxic evaluation had to be adjusted between the two sequences as

described in the "Treatments" section above. Statistical analysis for synergism was conducted independently for each sequence, with separate and appropriate controls for each of the two combination treatment schedules. To analyze the synergy, we fit a single ANCOVA model with indicators for carboplatin and for PDT, and the interaction between these variables was the basis for assessing the effect of the combination above that of the additive effects of each treatment alone. All analyses were performed on the log-transformed variables (of proportion viable and of tumor volume), so the parameter associated with the difference of treatment versus control (from the ANCOVA) was then exponentiated to summarize the impact of treatment on each of these measures of outcome. As a result of this, the confidence intervals will not be symmetric about the mean. Analyses were performed separately for each sequence.

RESULTS

Model Development and Size Characterization

OVCAR5 cells overlaid as a single cell suspension on a bed of GFR-Matrigel™ spontaneously formed 3D multicellular tumor nodules resembling adherent micrometastatic disease (Figures 1A-D). Ten days after plating, the 3D micronodules demonstrated cell surface and intracellular punctate E-cadherin expression (Figure 1B), a distribution pattern associated with metastatic ovarian tumors (3, 38). Micronodules were also encapsulated in a basement membrane containing human fibronectin (Figure 1C), a marker correlated with metastatic, chemoresistant and recurrent disease, indicating the poorest outcome for OvCa patients (39, 40). Migration, assembly and proliferation events (Supplementary movie S1) led to heterogeneous 3D nodules resembling micrometastatic disease within 11 days of plating (Figure 1D). The micronodules grew from a mean diameter of 34.3μm (± 2.6μm) 3 days post-plating (n = 9) to a mean diameter of 108.9μm (± 13.0μm) at day 10 (n = 9) and 131.9μm (± 25.3μm) at day 17 (n = 3) (Figure 1E).

Differential Response to Treatment with Carboplatin and PDT in Monolayer versus 3D

Cytotoxic response to escalating doses of carboplatin or PDT in 3D versus traditional monolayer cultures (Figures 2A and 2B) was evaluated by quantitative imaging of LIVE/DEAD reagents. Monolayer cultures significantly overestimate the sensitivity of OvCa cells to carboplatin treatment. At 40.0 mg/m^2 (one-tenth the clinically effective dose for intraperitoneally administered carboplatin) (41) OVCAR5 cells showed 3-fold higher sensitivity to carboplatin in monolayer than the same cells in 3D: 0.30 (± 0.082) fraction viability in monolayer, (n = 10), as compared to 0.90 (± 0.057) fraction viability in 3D, (n = 6) ($p < 0.001$, two-tailed t-test), relative to no treatment controls (n = 11 and 6 for monolayer and 3D, respectively) (Figure 2A).

At a PDT dose of 1.25μM·J/cm^2 (0.250μM BPD and 5.0J/cm^2 of 690nm light), the fraction viability in monolayer OVCAR5 cultures was 0.35 (± 0.04) (n = 12), relative to no treatment controls (n = 12) (FIGURE 2B). At the same PDT dose in 3D, the fraction viability was 0.75 (±0.04) (n = 13), relative to no treatment controls, (n = 16). These notable differences in viability indicate that OVCAR5 cells are more than twice as sensitive to BPD-PDT in monolayer as compared to the same cells in 3D cultures (p = 0.003, two-tailed t-test).

3D Model Reveals Differential Patterns of Cytotoxic Response for Carboplatin versus PDT

Close examination of cytotoxicity in 3D ovarian micronodules treated 10 days after plating with either carboplatin or PDT alone revealed distinct cell death patterns for the individual monotherapies (Figures 3A and 3B). A persistent population of viable surviving cores was observed following incubation with 400 mg/m^2 carboplatin. As shown in a representative nodule (Figure 3A), the ethidium bromide (dead) signal had a peak width of 15-20μm (full

width at half-maximum) on the periphery of carboplatin treated micronodules, which overlapped minimally with calcein green (live) fluorescence from the inner core of the same micronodule. This cytotoxicity pattern indicates the presence of a surviving core that was non-sensitive or impermeant to carboplatin.

Similar analysis of BPD-PDT treated micronodules revealed a contrasting cytotoxic pattern. Figure 3B shows a representative micronodule treated with 1.25μM·J/cm^2 BPD-PDT and fluorescence intensity profiles from two regions of interest in the micronodule. BPD-PDT disrupts micronodular structure and creates punctuate regions of highly overlapping calcein green and ethidium bromide fluorescence peaks.

Sequence-dependent synergistic reduction in viability and tumor burden in 3D micronodules treated with combination PDT and carboplatin

Based on the distinct cytotoxic mechanisms for carboplatin (8,23,41) versus BPD-PDT (4,27,29), and the differential cell death patterns observed here, we hypothesized that the two modalities could synergize to enhance efficacy at lower doses. We tested this hypothesis by treating the ovarian micronodules with low dose carboplatin (40 mg/m^2) either before or after 1.25μM·J/cm^2 BPD-PDT to determine the effect of treatment order.

Treatment with BPD-PDT prior to carboplatin, produced a significant synergistic reduction ($p < 0.0001$, interaction term from ANCOVA) in residual tumor volume and viability compared to the monotherapies, relative to no treatment ($n = 14$). Mean fraction residual tumor in the combination treatment group was 0.26 (95% CI=0.19-0.36, $n = 11$), as compared to 0.76 (95% CI=0.63-0.92, $n = 15$) with PDT alone and 0.95 (95% CI=0.83-1.09, $n = 11$) with carboplatin alone (Figure 4). Mean fraction viability in the combination PDT + carboplatin treated group was 0.45 (95% CI = 0.38 to 0.53, $n = 11$), as compared to PDT alone (0.80, 95% CI = 0.74 to 0.86, $n = 15$) or carboplatin alone (0.92, 95% CI = 0.88 to 0.97, $n = 11$) (Figure 5).

Conversely, no synergy was observed between the monotherapies with the reverse treatment order, carboplatin followed by BPD-PDT (Figure 6). Mean fraction residual tumor burden with either PDT alone or carboplatin alone was 0.61 (95% CI = 0.55 to 0.68, $n = 18$) and 0.64 (95% CI = 0.61 to 0.67, $n = 18$), respectively, relative to no treatment ($n = 18$) (Figure 6A). The discrepancy in treatment response in the carboplatin only arm between the two sequences (Figures 4/5 and Figure 6), is due to the adjustment in timepoint of evaluation necessitated by a fixed carboplatin schedule and duration as described in the Methods section. Compared to the monotherapies, the reverse combination treatment produced the most substantial decrease in mean fraction residual tumor burden (0.36, 95% CI = 0.34 to 0.39, $n = 18$) but this reduction was not synergistic ($p = 0.3326$, ANCOVA). Similarly, mean fraction viability in micronodules treated with either PDT alone or carboplatin alone was 0.78 (95% CI = 0.74 to 0.82, $n = 18$) and 0.79 (95% CI = 0.77 to 0.82, $n = 18$), respectively as compared to 0.65 (95% CI = 0.62 to 0.69, $n = 18$) in the combination carboplatin + PDT group, indicating no interaction between the two modalities ($p = 0.1368$, ANCOVA) (Figure 6B).

DISCUSSION

PDT has shown clinical promise for the treatment of disseminated OvCa (14-17,19), and will likely be most effective as part of a multifaceted treatment strategy to overcome resistance mechanisms that lead to treatment failure. The data presented in this study demonstrate a treatment-order dependent synergism with BPD-PDT and low-dose carboplatin using a 3D high-throughput reporter for adherent ovarian micrometastases.

Mechanistic differences between the individual modalities could account for the sequence-dependent synergism. Carboplatin is hydrolyzed as it enters a cell, creating an active species that forms interstrand and intrastrand DNA adducts. Depending on the extent of damage, the cell either enters cell cycle arrest or undergoes apoptosis, probably via ATM-CHK2 mediated activation of p53 in the nucleus (8,42). This triggers transcriptional upregulation of pro-apoptotic proteins Bax/Bak and downregulation of anti-apoptotic Bcl-2/Bcl-X_L in the cytosol, causing permeabilization of the outer mitochondrial membrane. Cytochrome *c* is subsequently released from the mitochondria followed by activation of caspase 9 and effector caspases 3,6 and 7, which triggers the apoptotic machinery that is responsible for DNA fragmentation and protein degradation typical of programmed cell death (8,23,41,42).

In contrast, BPD-PDT bypasses the nuclear signaling pathways that platinum agents rely on by damaging the mitochondrial membrane and initiating cytochrome *c*-mediated apoptosis or by directly destroying Bcl-2 associated with the mitochondria or endoplasmic reticulum (ER) (4,18,26,27,29,31). The observed synergism between the two modalities could, therefore, be explained by a combination of three possible mechanisms: 1) BPD-PDT is in itself cytotoxic to target cells and decreases the size of residual ovarian tumors. As recently quantified by Celli et al. (36), BPD-PDT shifts OvCa size distribution towards smaller nodules, in contrast to carboplatin, which had minimal impact on size reduction. These results could have important implications for designing more effective therapeutic regimens, since small OvCa nodules are associated with significantly better PFS, OS and response to chemotherapy than large tumors (5,41). 2) BPD-PDT also disrupts nodular architecture creating tumors that are more vulnerable to carboplatin. High cellular density is a critical barrier to the penetration, and accumulation, of chemotherapeutic agents in tumors (7). Treatment-induced apoptosis has specifically been shown to decrease cellular density and enhance the uptake of chemotherapies into tumor micronodules (7). Therefore, BPD-PDT mediated apoptotic disruption of micronodular architecture could play an important role in improving the delivery of platinum-based agents into residual OvCa nodules. This enhanced diffusion is particularly important within the context of intraperitoneal administration of carboplatin, which relies on surface penetration of the drug to achieve therapeutic benefit (41,43). 3) At the sub-cellular level, BPD-PDT sensitizes surviving cells to nuclear apoptotic signaling initiated by carboplatin, thereby lowering the threshold required to achieve a cytotoxic effect. The sequence-dependent synergism could therefore be driven by the ability of BPD-PDT to reduce the size and disrupt the structure of ovarian micronodules, in addition to sensitizing the cells to apoptotic signals from carboplatin treatment. Additional studies are necessary to elucidate the mechanisms for the observed synergism and to cross-validate these findings with tumor regrowth in 3D as well as focused *in vivo* and patient tissue experiments.

The applicability of these findings to a broader library of photosensitizers and chemotherapies needs to considered within the context of cytotoxic mechanisms. PDT-induced cellular damage can trigger a combination of non-specific necrosis, apoptosis, or autophagy (18,21). The predominance of a particular cytotoxic pathway depends on a variety of factors including the photophysical properties and preferred localization (and re-localization) sites of a photosensitizer, the local microenvironment, the fluence rate and PDT-dose, as well as compensatory survival mechanisms (18,21,24-29). BPD, mesochlorin, and aluminum (III) phthalocyanine tetrasulfonate chloride (AlPcS(4)) localize primarily to the mitochondria, and are efficient inducers of apoptosis (24,26,27,29). A more complex response is observed with photosensitizers that localize to the ER such as AlPcCl, and 9-capronyloxytetrakis (methoxyethyl) porphycene (CPO) (18). Depending on the PDT-dose, autophagy can be induced as either a pro-survival or pro-death pathway, which could be important in cells with defective apoptotic machinery, or resistance to apoptotis, and should be considered in mechanism-based combination regimens.

A variety of photosensitizers have been studied for PDT-mediated potentiation of chemotherapeutic agents including Photofrin, Photofrin II, delta-aminolevulinic acid (5-ALA), mesochlorin e_6 monoethylene diamine (Mce_6), meta-tetra(hydroxyphenyl)chlorin (m-THPC, Foscan), and indocyanine green (ICG) (21). The chemotherapeutic agents evaluated were cisplatin, doxorubicin and mytomicin C, which mediate cell death via DNA adducts (21). PDT in combination with these pharmacological therapies was shown to enhance tumor destruction and reduce toxicity compared to chemotherapy alone (21). The optimal treatment sequence, however, was dependent on the photosensitizer and chemotherapeutic agents that were used. Cisplatin cytotoxicity was enhanced most significantly when the chemotherapeutic was administered before Photofrin or ICG-based PDT. Similarly, the strongest potentiation of mitomycin C efficacy was seen when the drug was delivered prior to Photofrin II or 5-ALA-mediated PDT. Conversely, doxorubicin was most effective after treatment with Photofrin II, Mce_6 or m-THPC-based PDT.

The *in vitro* 3D platform for micrometastatic OvCa described here fills a critical niche in translational science by bridging the gap between resource-intensive animal models and traditional monolayer cultures that lack important determinants of tumor growth and treatment response. Consistent with previous findings (12,44), our results indicate that traditional monolayer cultures significantly overestimate the sensitivity of OvCa cells to cytotoxic treatments, which limits their value as tools to evaluate therapeutic efficacy. In contrast, tumor reduction in the same cells grown in 3D culture was comparable to results from *in vivo* studies (4,31), which demonstrated that, as in the present study, multiple rounds of BPD-PDT or rationally-designed combinations were necessary to achieve significant therapeutic benefit. An additional strength of the 3D platform is the demonstrated ability to evaluate dosing schedules over a time period that more closely mimics *in vivo* experiments than monolayer cultures. High resolution longitudinal imaging of cytotoxicity in the 3D platform also reveals differential cytotoxic patterns for carboplatin and BPD-PDT on a nodule-by-nodule basis that would be impossible to uncover in monolayer. These capabilities, combined with a system for high-throughput screening, facilitate rapid optimization of treatment parameters and allow valuable resources for *in vivo* and patient tissue studies to be focused on the most promising regimens.

The treatment response factors addressed by this system include interaction of the monotherapies at the sub-cellular level and architectural disruption of ovarian nodules by BPD-PDT suggesting improved delivery of carboplatin. Future models will incorporate more complex aspects of the tumor microenvironment including co-cultures with stromal partners including fibroblasts and endothelial cells. These co-cultures are motivated in part by clinical findings from Menon et. al. (45), who showed that nodules as small as 1mm (the smallest evaluated in the study) showed evidence of vascularity in peritoneal malignancies, including ovarian carcinomatosis. As the authors suggest, it was not clear if the vasculature in the smallest nodules was functional or even properly organized (45). It is important to explore whether endothelial cells, as signaling partners, have an impact on tumor growth or treatment response, even in the absence of flow or structural organization. New *in vitro* models for ovarian micrometastases using customizable matrices and stromal cells are being investigated by our group (46) and others (47,48), and will play an increasingly important role in screening combination regimens and uncovering resistance mechanisms.

Within the context of designing effective multifaceted treatments for OvCa, PDT-based combination regimens have been shown to reverse cisplatin resistance (13), to synergistically increase the therapeutic effect of targeted biological therapies (4), and now to synergistically enhance carboplatin efficacy for the treatment of multifocal OvCa. These findings are particularly significant in view of the fact that the highly toxic therapies

currently used to treat metastatic OvCa have produced only modest improvements in the recurrence rates and mortality associated with this disease.

In an effort to address this challenge of a narrow therapeutic window, we used doses of BPD-PDT and carboplatin in this study that were substantially lower than the typical range used *in vivo* and in the clinic (24,41,43,49,50). Keeping in mind the need for well-tolerated treatments, tumor destruction could be further improved with incremental and concomitant increases in the doses of both monotherapies. This approach will likely be more successful than significantly increasing either monotherapy to higher and more toxic levels. Also, in contrast to carboplatin (23,41,43), PDT can be administered in multiple rounds without additive host toxicity (4,31). This attribute, along with PDT's ability to sensitize chemoresistant and chemosensitive OvCa nodules to platinum-based agents (13), highlights the need to explore the effect of repeatedly treating 3D micronodules with low-dose BPD-PDT in combination with low-dose carboplatin. The high throughput capabilities of the platform described here can be harnessed to evaluate these additional treatment scenarios, and to inform focused pre-clinical experiments.

The results and strategies presented here could be used to design more effective and well-tolerated clinical combination regimens, based on previously published studies using PDT to treat a variety of disseminated peritoneal malignancies, including ovarian carcinomatosis (14-19). Phase I and II PDT clinical trials using non-optimized treatment parameters and Photofrin, have shown promise in treating cytoreduced minimal residual disease and chemoresistant peritoneal tumors (17). Photofrin-PDT conferred a survival advantage relative to historic controls with acute but reversible toxicities. Furthermore, OvCas were among the most responsive intra-abdominal solid tumors to intraperitoneal PDT (17). Building on these promising findings, we predict that BPD-PDT (which offers significant pharmacokinetic and photobiologic advantages over early generation photosensitizers) (4,29-31) in combination with low-dose carboplatin will be an effective and well-tolerated combination regimen.

Collectively, these preclinical and clinical reports indicate that PDT should be included in the regular armamentarium used to treat ovarian carcinomatoses as part of a comprehensive treatment plan designed to minimize toxicity with optimal cytoreductive effects. We envision a scenario in which BPD-PDT is used in conjunction with cytoreductive surgery to treat and sensitize unresectable tumors to chemo-, radio- and biological therapeutics. Due to the vast library of candidate interventions, high-throughput 3D treatment response platforms, as presented here, will play a critical role in selecting the appropriate combination regimens for multifocal OvCa as well as many other lethal metastatic cancers.

Supplementary Material

Refer to Web version on PubMed Central for supplementary material.

Acknowledgments

This work was supported by: NIH (RO1CA119388, RO1CA146337 and RO1AR040532 to TH), WCP Graduate Student Fellowship (IR), MBRC Tosteson Fellowship and NCI F32CA138153 (CLE).

ABBREVIATIONS

3D	Three-dimensional
5-ALA	Delta-aminolevulinic acid

AlPcS(4)	Aluminum (III) phthalocyanine tetrasulfonate chloride
BPD-MA	Benzoporphyrin derivative monoacid ring A
CI	Confidence Interval
ER	Endoplasmic reticulum
FDA	Food and Drug Administration
GFR	Growth factor reduced
ICG	Indocyanine green
Mce_6	Mesochlorin e_6 monoethylene diamine
m-THPC	Meta-tetra(hydroxyphenyl)chlorin
OS	Overall survival
OvCa	Ovarian cancer
PDT	Photodynamic therapy
PFS	Progression-free survival
PIT	Photoimmunotherapy

REFERENCES

1. BAST RC JR. HENNESSY B, MILLS GB. THE BIOLOGY OF OVARIAN CANCER: NEW OPPORTUNITIES FOR TRANSLATION. NAT REV CANCER 2009;9:415–28. [PubMed: 19461667]
2. CHO KR, SHIH IEM. OVARIAN CANCER. ANNUAL REVIEW OF PATHOLOGY 2009;4:287–313.
3. NAORA H, MONTELL DJ. OVARIAN CANCER METASTASIS: INTEGRATING INSIGHTS FROM DISPARATE MODEL ORGANISMS. NAT REV CANCER 2005;5:355–66. [PubMed: 15864277]
4. DEL CARMEN MG, RIZVI I, CHANG Y, et al. SYNERGISM OF EPIDERMAL GROWTH FACTOR RECEPTOR-TARGETED IMMUNOTHERAPY WITH PHOTODYNAMIC TREATMENT OF OVARIAN CANCER IN VIVO. JNCI 2005;97:1516–24. [PubMed: 16234565]
5. CHI DS, EISENHAUER EL, ZIVANOVIC O, et al. IMPROVED PROGRESSION-FREE AND OVERALL SURVIVAL IN ADVANCED OVARIAN CANCER AS A RESULT OF A CHANGE IN SURGICAL PARADIGM. GYNECOL ONCOL 2009;114:26–31. [PubMed: 19395008]
6. MINCHINTON AI, TANNOCK IF. DRUG PENETRATION IN SOLID TUMOURS. NAT REV CANCER 2006;6:583–92. [PubMed: 16862189]
7. AU JL, JANG SH, ZHENG J, et al. DETERMINANTS OF DRUG DELIVERY AND TRANSPORT TO SOLID TUMORS. J CONTROL RELEASE 2001;74:31–46. [PubMed: 11489481]
8. AGARWAL R, KAYE SB. OVARIAN CANCER: STRATEGIES FOR OVERCOMING RESISTANCE TO CHEMOTHERAPY. NAT REV CANCER 2003;3:502–16. [PubMed: 12835670]
9. MARTIN LP, SCHILDER RJ. MANAGEMENT OF RECURRENT OVARIAN CARCINOMA: CURRENT STATUS AND FUTURE DIRECTIONS. SEMIN ONCOL 2009;36:112–25. [PubMed: 19332246]
10. GUARNERI V, PIACENTINI F, BARBIERI E, CONTE PF. ACHIEVEMENTS AND UNMET NEEDS IN THE MANAGEMENT OF ADVANCED OVARIAN CANCER. GYNECOLOGIC ONCOLOGY 2010;117:152–8. [PubMed: 20056266]
11. GRIFFITH LG, SWARTZ MA. CAPTURING COMPLEX 3D TISSUE PHYSIOLOGY IN VITRO. NATURE REVIEWS MOLECULAR CELL BIOLOGY 2006;7:211–24.

12. SHARMA SV, HABER DA, SETTLEMAN J. CELL LINE-BASED PLATFORMS TO EVALUATE THE THERAPEUTIC EFFICACY OF CANDIDATE ANTICANCER AGENTS. NAT REV CANCER 2010;10:241–53. [PubMed: 20300105]
13. DUSKA LR, HAMBLIN MR, MILLER JL, HASAN T. COMBINATION PHOTOIMMUNOTHERAPY AND CISPLATIN: EFFECTS ON HUMAN OVARIAN CANCER EX VIVO. J NATL CANCER INST 1999;91:1557–63. [PubMed: 10491432]
14. HAHN SM, FRAKER DL, MICK R, et al. A PHASE II TRIAL OF INTRAPERITONEAL PHOTODYNAMIC THERAPY FOR PATIENTS WITH PERITONEAL CARCINOMATOSIS AND SARCOMATOSIS. CLINICAL CANCER RESEARCH 2006;12:2517. [PubMed: 16638861]
15. DELANEY TF, SINDELAR WF, TOCHNER Z, et al. PHASE I STUDY OF DEBULKING SURGERY AND PHOTODYNAMIC THERAPY FOR DISSEMINATED INTRAPERITONEAL TUMORS. INTERNATIONAL JOURNAL OF RADIATION ONCOLOGY, BIOLOGY, PHYSICS 1993;25:445–57.
16. SINDELAR WF, DELANEY TF, TOCHNER Z, et al. TECHNIQUE OF PHOTODYNAMIC THERAPY FOR DISSEMINATED INTRAPERITONEAL MALIGNANT NEOPLASMS. PHASE I STUDY. ARCH SURG 1991;126:318–24. [PubMed: 1998474]
17. HENDREN SK, HAHN SM, SPITZ FR, et al. PHASE II TRIAL OF DEBULKING SURGERY AND PHOTODYNAMIC THERAPY FOR DISSEMINATED INTRAPERITONEAL TUMORS. ANNALS OF SURGICAL ONCOLOGY 2001;8:65–71. [PubMed: 11206227]
18. KESSEL D, REINERS JJ JR. APOPTOSIS AND AUTOPHAGY AFTER MITOCHONDRIAL OR ENDOPLASMIC RETICULUM PHOTODAMAGE. PHOTOCHEM PHOTOBIOL 2007;83:1024–8. [PubMed: 17880495]
19. WIERRANI F, FIEDLER D, GRIN W, et al. CLINICAL EFFECT OF MESO-TETRAHYDROXYPHENYLCHLORINE BASED PHOTODYNAMIC THERAPY IN RECURRENT CARCINOMA OF THE OVARY: PRELIMINARY RESULTS. BR J OBSTET GYNAECOL 1997;104:376–8. [PubMed: 9091020]
20. GOMER CJ, FERRARIO A, LUNA M, RUCKER N, WONG S. PHOTODYNAMIC THERAPY: COMBINED MODALITY APPROACHES TARGETING THE TUMOR MICROENVIRONMENT. LASERS SURG MED 2006;38:516–21. [PubMed: 16607618]
21. ZULUAGA MF, LANGE N. COMBINATION OF PHOTODYNAMIC THERAPY WITH ANTI-CANCER AGENTS. CURR MED CHEM 2008;15:1655–73. [PubMed: 18673216]
22. HONGRAPIPAT J, KOPECKOVA P, LIU J, PRAKONGPAN S, KOPECEK J. COMBINATION CHEMOTHERAPY AND PHOTODYNAMIC THERAPY WITH FAB' FRAGMENT TARGETED HPMA COPOLYMER CONJUGATES IN HUMAN OVARIAN CARCINOMA CELLS. MOL PHARM 2008;5:696–709. [PubMed: 18729468]
23. MARKMAN M. PHARMACEUTICAL MANAGEMENT OF OVARIAN CANCER : CURRENT STATUS. DRUGS 2008;68:771–89. [PubMed: 18416585]
24. CELLI JP, SPRING BQ, RIZVI I, et al. IMAGING AND PHOTODYNAMIC THERAPY: MECHANISMS, MONITORING, AND OPTIMIZATION. CHEM REV 2010;110:2795–838. [PubMed: 20353192]
25. DOUGHERTY TJ, GOMER CJ, HENDERSON BW, et al. PHOTODYNAMIC THERAPY. J NATL CANCER INST 1998;90:889–905. [PubMed: 9637138]
26. HASAN, T.; ORTEL, B.; SOLBAN, N.; POGUE, B. PHOTODYNAMIC THERAPY OF CANCER. In: KUFE, DW.; BAST, RCJ.; HAIT, WN., et al., editors. CANCER MEDICINE. 7TH ED. B.C. DECKER, INC.; HAMILTON, ONTARIO: 2006. p. 537-48.
27. KESSEL D, CASTELLI M. EVIDENCE THAT BCL-2 IS THE TARGET OF THREE PHOTOSENSITIZERS THAT INDUCE A RAPID APOPTOTIC RESPONSE. PHOTOCHEMISTRY AND PHOTOBIOLOGY 2001;74:318–22. [PubMed: 11547571]
28. WILSON BC. PHOTODYNAMIC THERAPY FOR CANCER: PRINCIPLES. CAN J GASTROENTEROL 2002;16:393–6. [PubMed: 12096303]
29. GRANVILLE DJ, JIANG H, AN MT, LEVY JG, MCMANUS BM, HUNT DW. BCL-2 OVEREXPRESSION BLOCKS CASPASE ACTIVATION AND DOWNSTREAM APOPTOTIC

EVENTS INSTIGATED BY PHOTODYNAMIC THERAPY. BR J CANCER 1999;79:95–100. [PubMed: 10408699]

30. AVELINE B, HASAN T, REDMOND RW. PHOTOPHYSICAL AND PHOTOSENSITIZING PROPERTIES OF BENZOPORPHYRIN DERIVATIVE MONOACID RING A (BPD-MA). PHOTOCHEM PHOTOBIOL 1994;59:328–35. [PubMed: 8016212]
31. MOLPUS KL, KATO D, HAMBLIN MR, LILGE L, BAMBERG M, HASAN T. INTRAPERITONEAL PHOTODYNAMIC THERAPY OF HUMAN EPITHELIAL OVARIAN CARCINOMATOSIS IN A XENOGRAFT MURINE MODEL. CANCER RES 1996;56:1075–82. [PubMed: 8640764]
32. NIH. REPORT EXPENDITURES AND RESULTS (REPORTER). ENHANCING DIRECT TUMOR CELL CYTOTOXICITY BY MANIPULATING GROWTH FACTOR SIGNALING. [CITED 2010 MARCH 17]. 2010 AVAILABLE FROM: HTTP://PROJECTREPORTER.NIH.GOV/PROJECT_INFO_DESCRIPTION.CFM?AID=7971200&ICDE=2703496
33. LURJE G, LENZ HJ. EGFR SIGNALING AND DRUG DISCOVERY. ONCOLOGY 2009;77:400–10. [PubMed: 20130423]
34. PETERSEN OW, RONNOV-JESSEN L, HOWLETT AR, BISSELL MJ. INTERACTION WITH BASEMENT MEMBRANE SERVES TO RAPIDLY DISTINGUISH GROWTH AND DIFFERENTIATION PATTERN OF NORMAL AND MALIGNANT HUMAN BREAST EPITHELIAL CELLS. PROC NATL ACAD SCI U S A 1992;89:9064–8. [PubMed: 1384042]
35. DEBNATH J, MUTHUSWAMY SK, BRUGGE JS. MORPHOGENESIS AND ONCOGENESIS OF MCF-10A MAMMARY EPITHELIAL ACINI GROWN IN THREE-DIMENSIONAL BASEMENT MEMBRANE CULTURES. METHODS 2003;30:256–68. [PubMed: 12798140]
36. CELLI JP, RIZVI I, EVANS CL, ABU-YOUSIF AO, HASAN T. QUANTITATIVE IMAGING REVEALS HETEROGENEOUS GROWTH DYNAMICS AND TREATMENT-DEPENDENT RESIDUAL TUMOR DISTRIBUTIONS IN A 3D OVARIAN CANCER MODEL. J BIOMED OPTICS 2010;15: PIONEERS IN BIOMEDICAL OPTICS: SPECIAL SECTION HONORING PROFESSOR TAYYABA HASAN
37. EVANS CL, RIZVI I, HASAN T, DE BOER JF. IN VITRO OVARIAN TUMOR GROWTH AND TREATMENT RESPONSE DYNAMICS VISUALIZED WITH TIME-LAPSE OCT IMAGING. OPT EXPRESS 2009;17:8892–906. [PubMed: 19466138]
38. SUNDFELDT K. CELL-CELL ADHESION IN THE NORMAL OVARY AND OVARIAN TUMORS OF EPITHELIAL ORIGIN; AN EXCEPTION TO THE RULE. MOL CELL ENDOCRINOL 2003;202:89–96. [PubMed: 12770736]
39. DEMETER A, SZILLER I, CSAPO Z, et al. MOLECULAR PROGNOSTIC MARKERS IN RECURRENT AND IN NON-RECURRENT EPITHELIAL OVARIAN CANCER. ANTICANCER RES 2005;25:2885–9. [PubMed: 16080542]
40. FRANKE FE, VON GEORGI R, ZYGMUNT M, MUNSTEDT K. ASSOCIATION BETWEEN FIBRONECTIN EXPRESSION AND PROGNOSIS IN OVARIAN CARCINOMA. ANTICANCER RES 2003;23:4261–7. [PubMed: 14666636]
41. FUJIWARA K. CAN CARBOPLATIN REPLACE CISPLATIN FOR INTRAPERITONEAL USE? INT J GYNECOL CANCER 2008;18(SUPPL 1):29–32. [PubMed: 18336396]
42. ASHKENAZI A. TARGETING THE EXTRINSIC APOPTOSIS PATHWAY IN CANCER. CYTOKINE GROWTH FACTOR REV 2008;19:325–31. [PubMed: 18495520]
43. MARKMAN M. INTRAPERITONEAL CHEMOTHERAPY IN THE MANAGEMENT OF OVARIAN CANCER: FOCUS ON CARBOPLATIN. THER CLIN RISK MANAG 2009;5:161–8. [PubMed: 19436618]
44. OHMORI T, YANG JL, PRICE JO, ARTEAGA CL. BLOCKADE OF TUMOR CELL TRANSFORMING GROWTH FACTOR-BETAS ENHANCES CELL CYCLE PROGRESSION AND SENSITIZES HUMAN BREAST CARCINOMA CELLS TO CYTOTOXIC CHEMOTHERAPY. EXPERIMENTAL CELL RESEARCH 1998;245:350–9. [PubMed: 9851876]
45. MENON C, KUTNEY SN, LEHR SC, et al. VASCULARITY AND UPTAKE OF PHOTOSENSITIZER IN SMALL HUMAN TUMOR NODULES: IMPLICATIONS FOR

INTRAPERITONEAL PHOTODYNAMIC THERAPY. CLIN CANCER RES 2001;7:3904–11. [PubMed: 11751481]

46. ABU-YOUSIF AO, RIZVI I, EVANS CL, CELLI JP, HASAN T. PURAMATRIX ENCAPSULATION OF CANCER CELLS. JOURNAL OF VISUALIZED EXPERIMENTS. DECEMBER 17.2009 AVAILABLE FROM: HTTP://WWW.JOVE.COM/INDEX/DETAILS.STP?ID=1692.
47. KENNY HA, KRAUSZ T, YAMADA SD, LENGYEL E. USE OF A NOVEL 3D CULTURE MODEL TO ELUCIDATE THE ROLE OF MESOTHELIAL CELLS, FIBROBLASTS AND EXTRA-CELLULAR MATRICES ON ADHESION AND INVASION OF OVARIAN CANCER CELLS TO THE OMENTUM. INT J CANCER 2007;121:1463–72. [PubMed: 17546601]
48. BURLESON KM, BOENTE MP, PAMBUCCIAN SE, SKUBITZ AP. DISAGGREGATION AND INVASION OF OVARIAN CARCINOMA ASCITES SPHEROIDS. JOURNAL OF TRANSLATIONAL MEDICINE 2006;4:6. [PubMed: 16433903]
49. PEREIRA, SP. OPTICAL METHODS FOR TUMOR TREATMENT AND DETECTION: MECHANISMS AND TECHNIQUES IN PHOTODYNAMIC THERAPY XVIII. SPIE; SAN JOSE, CA, USA: 2009. PHOTODYNAMIC THERAPY FOR PANCREATIC AND BILIARY TRACT CARCINOMA; p. 71640J-10.2009
50. LEWIS, R.; SCHUMAN, L.; MICKLER, M., et al. PRECLINICAL EVALUATION OF CETUXIMAB AND BENZOPORPHYRIN DERIVATIVE-MEDIATED INTRAPERITONEAL PHOTODYNAMIC THERAPY IN A CANINE MODEL. 35TH MEETING OF THE AMERICAN SOCIETY FOR PHOTOBIOLOGY; BROWN UNIVERSITY, PROVIDENCE, RI: AMERICAN SOCIETY FOR PHOTOBIOLOGY. 2010. p. 34

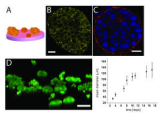

Figure 1.

Biological characterization of a 3D model for micrometastatic OvCa. A, OVCAR5 cells overlaid on GFR-Matrigel™ formed 3D ovarian micronodules representing adherent micrometastatic disease with B, punctate E-cadherin expression, and C, fibronectin (red) expression (blue: DAPI), markers for poor prognosis. D, mean diameter increased from 34.3μm (±2.6μm) 3 days post-plating (n = 9) to 108.9μm (± 13.0μm) at day 10 (n = 9) and 131.9μm (±25.3μm) at day 17 (n = 3) (E). Scale bars: (B) and (C), 20μm; (D) 150μm.

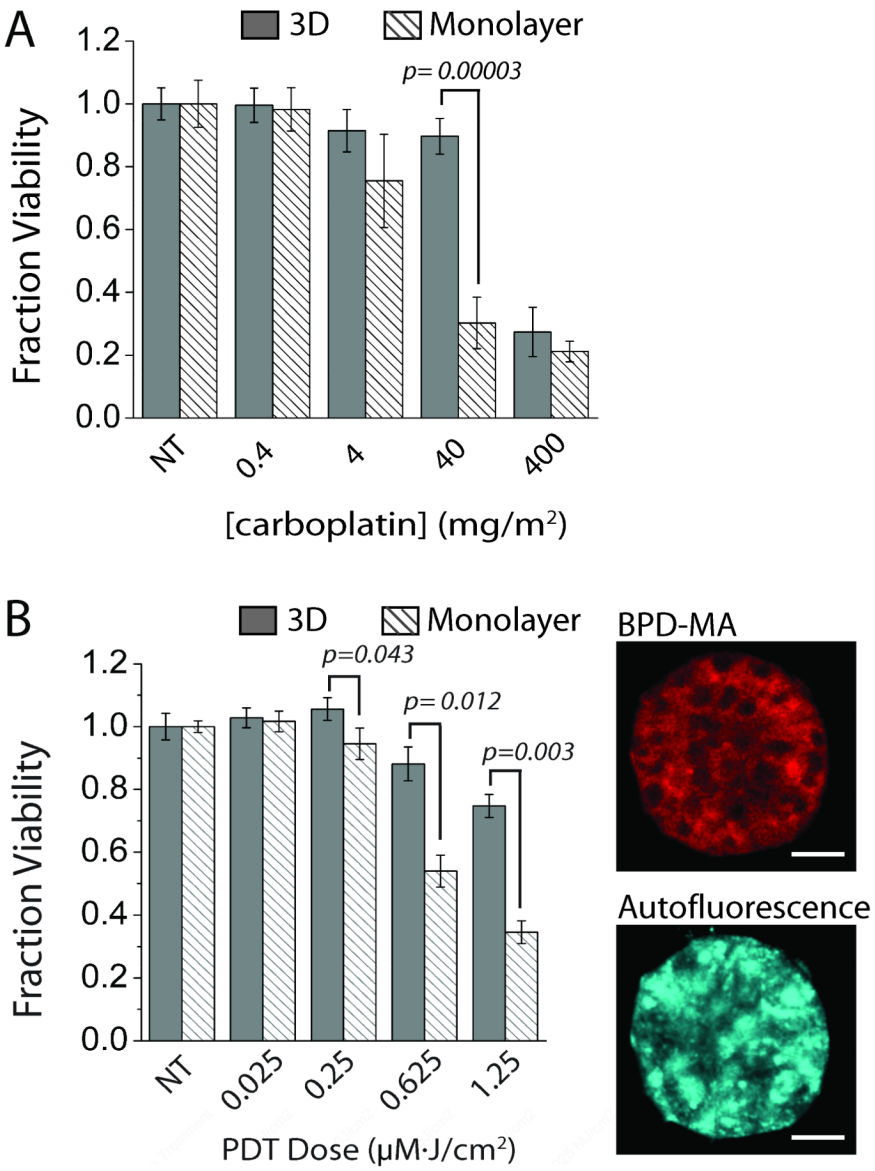

Figure 2.

Monolayer cultures significantly overestimate carboplatin and BPD-PDT efficacy compared to cells in 3D. A, fractional viability of OVCAR5 cells in monolayer (striped) following carboplatin treatment (40 mg/m^2) was 0.30 (± 0.082) (n = 10), as compared to 0.90 (± 0.057) in 3D (solid), (n = 6) (p < 0.001, two-tailed t-test). B, left, monolayer cultures treated with 1.25μM·J/cm^2 BPD-PDT, had a fractional viability of 0.35 (± 0.04) (n = 12), as compared to 0.75 (±0.04) in 3D (n = 13) (p = 0.003, two-tailed t-test). N-values vary from 6 to 16 for individual treatment groups within each culture condition. B, right, confocal fluorescence images show BPD-MA distribution and autofluorescence from a representative nodule. Scale bars = 25μm.

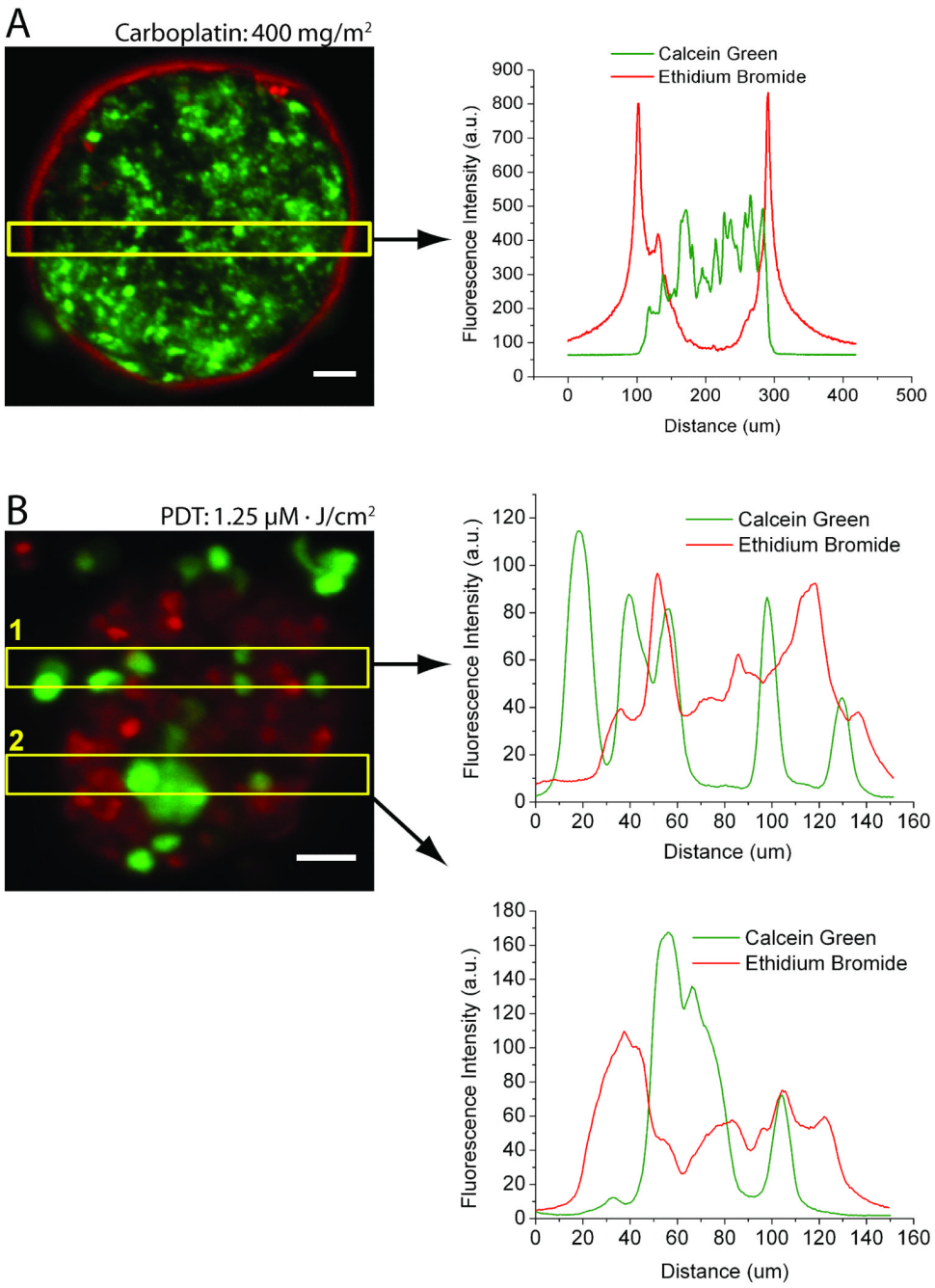

Figure 3.

Differential patterns of cytotoxic response in carboplatin and BPD-PDT treated 3D micronodules. A, left, a representative micronodule treated with 400 mg/m^2 carboplatin showing cell death (ethidium bromide) on the periphery of a viable (calcein) tumor core, with A, right, distinct and minimally overlapping fluorescence intensity profiles. B, left, BPD-PDT 1.25μM·J/cm^2 treatment leads to nodular disruption and punctate cytoxicity. B, right, intensity profile scans through two regions of interest (yellow boxes) show highly overlapping fluorescence patterns. Scale bars = 25μm.

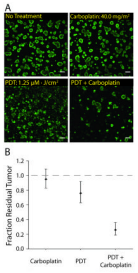

Figure 4.

BPD-PDT synergizes with low-dose carboplatin to reduce residual tumor volume. A, images of residual disease (calcein). B, fraction residual tumor following carboplatin alone or BPD-PDT alone was 0.95 (95% CI=0.83-1.09, n = 11) and 0.76 (95% CI=0.63-0.92 n = 15), respectively, relative to no treatment (grey dashed line). The combination treatment, BPD-PDT followed by carboplatin, produced a synergistic reduction in residual tumor to 0.26 (95% CI=0.19-0.36, n = 11) (p<0.0001, interaction term from ANCOVA). Scale bars = 250μm.

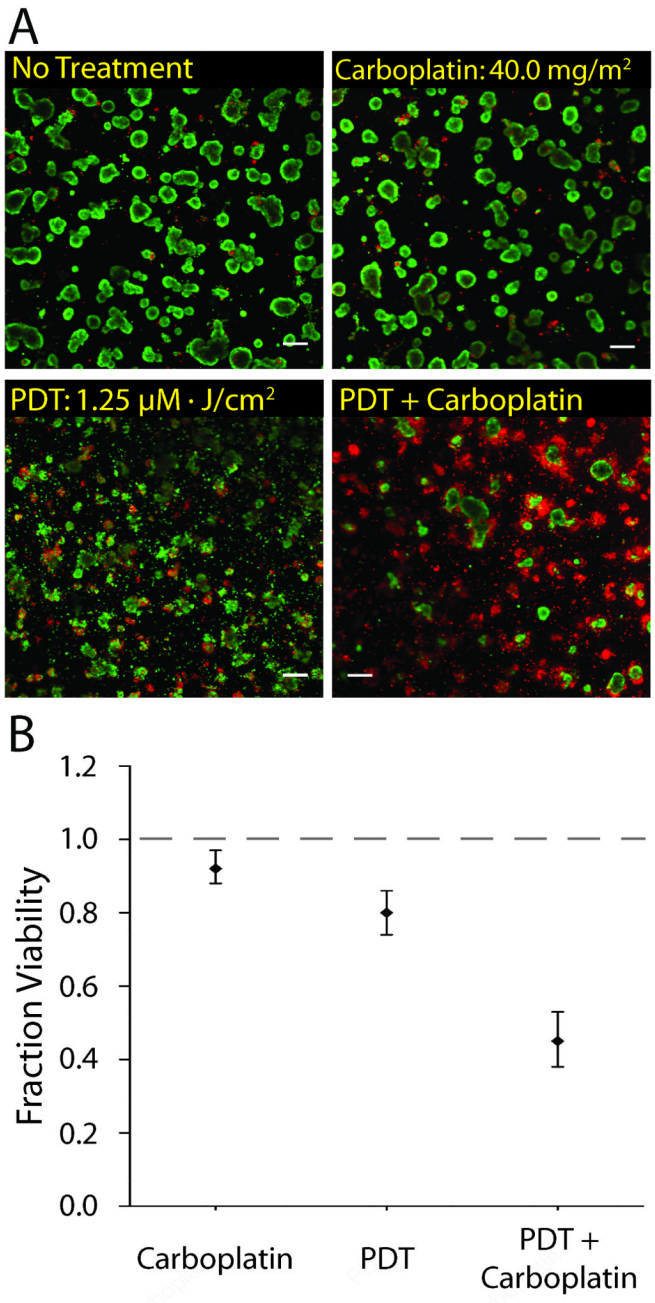

Figure 5.

BPD-PDT followed by carboplatin synergistically reduces tumor viability. A, images of tumor viability (calcein and ethidium bromide fluorescence) following treatment. B, mean fraction viability in micronodules treated with either carboplatin alone or BPD-PDT alone was 0.92 (95% CI=0.88-0.97, n = 11) and 0.80 (95%CI=0.74-0.86, n = 15), respectively, relative to no treatment (grey dashed line). The combination treatment, BPD-PDT followed by carboplatin, reduced viability to 0.45 (95% CI=0.38-0.53, n = 11), indicating a significant synergism (p<0.0001, interaction term from ANCOVA). Scale bars = 250μm.

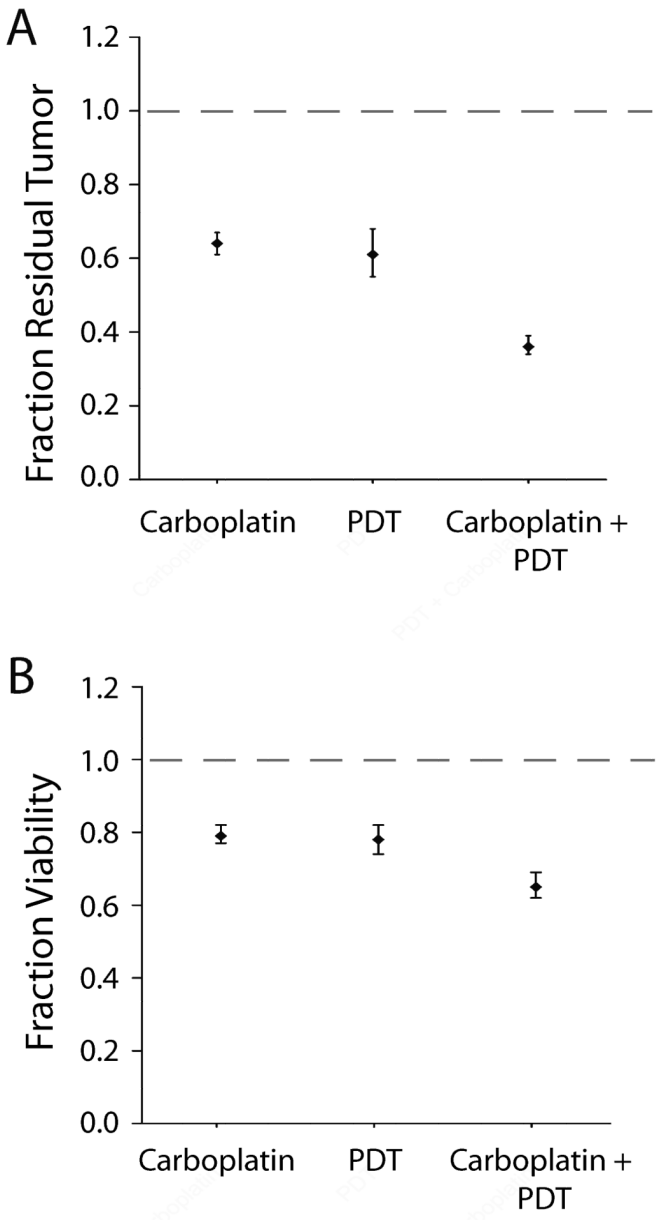

Figure 6.
Carboplatin treatment prior to BPD-PDT does not produce a synergistic interaction. No synergism was observed with the reverse treatment order, as evaluated by fraction of residual tumor (A) (p=0.3326), and tumor viability (B) (p=0.1368) (interaction term from ANCOVA for both treatment response metrics), relative to no treatment (grey dashed lines).